Pt^{IV}-Containing Hexaplatinate(II) $[Pt^{IV}Pt^{II}_6O_6(AsO_2(CH_3)_2)_6]^{2-}$ and Hexapalladate(II) $[Pt^{IV}Pd^{II}_6O_6(AsO_2(CH_3)_2)_6]^{2-}$

Jiayao Zhang,[a] Saurav Bhattacharya,[a,b] Bahaa E. Khsara,[a] Talha Nisar,[a] Anja B. Müller,[a] Maria Besora,[c] Josep M. Poblet,[c] Veit Wagner,[a] Nikolai Kuhnert,[a] and Ulrich Kortz[a,*]

Delicated to Prof. Achim Müller and Prof. Andre Tézé on the occasion of their 85th birthday

ABSTRACT: The first Pt^{IV}-containing discrete polyoxoplatinate(II) $[Pt^{IV}Pt^{II}_6O_6(AsO_2(CH_3)_2)_6]^{2-}$ (**Pt_7**) and polyoxopalladate(II) $[Pt^{IV}Pd^{II}_6O_6(AsO_2(CH_3)_2)_6]^{2-}$ (**$PtPd_6$**) have been prepared and characterized in the solid-state, in solution, and in the gas phase. The molecular structures of the noble metal-oxo clusters **Pt_7** and **$PtPd_6$** comprise a central, octahedral $Pt^{IV}O_6$ hetero group surrounded by six square-planar MO_4 (M = Pt^{II}, Pd^{II}) units, which are capped by six dimethylarsinate ligands. The polyanions were prepared in simple one-pot aqueous solution conditions by reacting $H_2Pt(OH)_6$ with either K_2PtCl_4 or $Pd(NO_3)_2$ in sodium dimethylarsinate buffer (pH 7) at 80 °C. Catalytic studies were performed on **Pt_7** supported on SBA15-apts for *o*-xylene hydrogenation at 300 °C and 90 bar H_2 pressure and indicated excellent activity and recyclability with low activation temperature.

INTRODUCTION

Polyoxometalates (POMs) are discrete and soluble polynuclear metal-oxo cluster anions, typically formed by edge- or corner-shared MO_6 octahedra where M is usually an early *d*-block metal ion in a high oxidation state (e.g. W^{VI}, Mo^{VI}, V^{V}, Nb^{V}, Ta^{V}).[1] POMs or POM-based materials are of interest in analytical chemistry (e.g. microscope staining), catalysis (supported heterogeneous oxidations, biologically relevant reactions, CO_2 reduction, water splitting, photo-/electrocatalytic reactions), biochemistry, medicine (antibacterial, antitumoral, antiviral activity), and solid-state devices (memory devices, energy production and storage).[2] In view of Döbereiner's idea that structurally well-defined noble metal-oxo clusters could serve as ideal models to decode the molecular mechanism of noble-metal-based catalysis,[3] an important milestone was the discovery of polyoxo-12-platinate(III) (POPt), $[Pt^{III}_{12}O_8(SO_4)_{12}]^{4-}$, by Wickleder and co-workers in 2004, which is the only polyoxoplatinate known till date.[4a] In 2022, the first polythioplatinate(II), $[Pt^{II}_3S_2(SO_3)_6]^{10-}$, was synthesized by the Kortz group.[4b] The first polyoxopalladate(II) (POPd), $[H_6Pd^{II}_{13}O_8(AsO_4)_8]^{8-}$, and the first polyoxoaurate(III) (POAu), $[Au^{III}_4O_4(AsO_4)_4]^{8-}$, were discovered by Kortz and co-workers in 2008 and 2010, respectively, which eventually led to the discovery of a large family of POPds with different shapes, sizes and compositions.[5] Recently, the first neutral palladium(II)-oxo clusters (POCs) were reported by Kortz and co-workers, such as the disk-shaped $[Pd_{16}O_8(OH)_8((CH_3)_2AsO_2)_8]$ (Pd_{16}) and its chloro-derivative $[Pd_{16}O_8(OH)_5Cl_3((CH_3)_2AsO_2)_8]$ ($Pd_{16}Cl$), the larger, bicapped derivative $[Pd_{24}O_{12}(OH)_8((CH_3)_2AsO_2)_{16}]$ (Pd_{24}) and the even larger $[Pd_{40}O_{24}(OH)_{16}(CH_3)_2AsO_2)_{16}]$ (Pd_{40}).[6] Even more recently, Kortz and co-workers discovered the first two examples of cationic POCs containing *f*-metal ions, $[Pd^{II}_6O_{12}M_8\{(CH_3)_2AsO_2\}_{16}(H_2O)_8]^{4+}$ (M = Ce^{IV}, Th^{IV}).[7] Although, the classical coordination chemistry of platinum has a long history and is replete with interesting compounds, only limited work has been reported on the coordination of Pt^{IV} or Pt^{II} to POMs. For example, in the 1990s oxonitro-complexes comprising di- and/or tetravalent platinum ions (e.g. $[Pt^{IV}Pt^{II}_3O_3(NO_2)_9]^{5-}$, $[Pt^{IV}Pt^{II}_6O_6(NO_2)_{12}]^{8-}$) were reported.[8] In 2015 polynuclear hydroxido-bridged platinum(IV) nitrato complexes, $[Pt^{IV}_4(OH)_6(NO_3)_{10}]$ and $[Pt^{IV}_6(OH)_{10}(NO_3)_{12}]^{2+}$, were reported.[9] In POM chemistry, Pt^{IV} was shown to act as a central hetero atom in Anderson-Evans-type hexatungstate and hexamolybdate with various degrees of protonation.[10] In 2008, the platinum(IV)-containing decavanadate $[H_2Pt^{IV}V_9O_{28}]^{5-}$ was prepared and structurally characterized.[11] The platinum(IV)-grafted

polyoxoniobate $[Nb_6O_{19}\{Pt(OH)_2\}]_2^{12-}$ was reported in 2015.[12] To date, some examples of Pt^{II}-containing POMs have been reported, such as $[Pt_2(W_5O_{18})_2]^{8-}$,[13] $[\alpha\text{-}PW_{11}O_{39}(cis\text{-}Pt(NH_3)_2)_2]^{3-}$,[14] *anti*- and *syn*-$[Pt^{II}_2(\alpha\text{-}PW_{11}O_{39})_2]^{10-}$,[15] and $[\alpha\text{-}PW_{11}O_{39}\{cis\text{-}Pt^{II}(Me_2ppz)\}]^{5-}$ (Me_2ppz = *N*,*N*'-dimethylpiperazine).[16] Recently, the Kortz group has reported a Pd^{IV}-centered polyoxopalladate(II), $[Pd^{IV}Pd^{II}_6O_6((CH_3)_2AsO_2)_6]^{2-}$.[17] This result motivated us to try and prepare a mixed-valent platinum analogue, and possibly to develop the class of polyoxoplatinates further.

EXPERIMENTAL SECTION

General methods and materials. The elemental analyses were performed by Zentrallabor, Technische Universität Hamburg (TUHH), Am Schwarzenberg-Campus 1, 21073 Hamburg (Pt, Pd, As for **$PtPd_6$**) and Analytische Laboratorien, Industriepark Kaiserau (Haus Heidbruch), 51789 Lindlar, Germany (Pt, As, CHN for **Pt_7** and CHN for **$PtPd_6$**). The K and Na analyses were performed in house by atomic absorption (AA) spectroscopy carried out on a Varian SpectrAA 220 AA spectrometer. The crystal water content was determined by thermogravimetric analysis (TGA) on a TA Instruments Q600 device at a heating rate of 5 ºC min^{-1} under N_2 atmosphere (25–500 ºC). The TGA curves of freshly prepared **KNa-Pt_7** and **Na-$PtPd_6$** indicated initial weight losses (~25–150 ºC) of ~13.5% and ~7.8%, respectively, which correspond to the loss of the lattice water molecules (calculated ~12.7% for **KNa-Pt_7** and ~7.6% for **Na-$PtPd_6$**, respectively, see Figure S1). The second weight loss steps for **KNa-Pt_7** and **Na-$PtPd_6$** (~150–500 ºC) correspond to the overall decomposition of the POM skeleton. Fourier Transform Infrared spectra (FTIR, KBr pellets) were recorded on a Nicolet-Avatar 370 spectrometer (4000–400 cm^{-1}). The solution ^1H and ^{13}C NMR spectra were recorded on a JEOL ECS 400 MHz spectrometer using 5 mm tubes, and with resonance frequencies of 399.78 MHz and 100.71 MHz for ^1H and ^{13}C, respectively. The resonance frequency for ^{195}Pt NMR was 85.94 MHz and the chemical shifts are reported with respect to 1M Na_2PtCl_6 in H_2O/D_2O as 0 ppm reference. All measurements were performed at room temperature and by using H_2O/D_2O as the solvent.

High-resolution ESI-MS spectra were recorded using a Bruker Daltonics Q-TOF Impact instrument employing both negative and positive electrospray ionization modes. MicrOTOF Focus mass spectrometer (Bruker Daltonics) was fitted with an ESI source and external calibration was achieved with 10 mL of 0.1M sodium formate solution. The instrument ion source and tubing were rinsed with

methanol. The calibration was carried out using the enhanced quadratic calibration mode. All ESI-MS measurements were performed in both negative and positive ion modes. Samples were measured as direct infusions at a concentration of 100 µg/mL in deionized water at a flow rate of 180 µL/min. The spectral simulations were carried out in Data Analysis 4.1 (Bruker Daltonics, Bremen).

The oxidation states of Pt and Pd in **Pt_7** and **$PtPd_6$** were ascertained using X-ray photoelectron spectroscopy (XPS) measurements. The samples were dispersed in acetone and spin-coated onto the as prepared substrates at a rotation speed of 1000 rpm. The ultra-high vacuum vessel, which had a vacuum pressure of ~1 x 10^{-8} mbar, was equipped with a water-cooled X-ray gun with a double Mg/Al anode (Specs XR 50) and a hemispherical electron analyzer (Specs Phoibos 100). Mg $K\alpha_{1,2}$ radiation (E = 1253.6 eV) was used as a source of excitation. The photoelectrons were detected in the large area lens mode and fixed analyzer transmission at a pass energy of 50 eV. The measured data were analyzed using the CASA-XPS software. The positions of the peaks were in the expected regions.

X-ray crystallography. Data for **KNa-Pt_7** were collected at 100 K on a Bruker D8 APEX II CCD single-crystal diffractometer equipped with kappa geometry (graphite monochromator, $\lambda_{Mo\ K\alpha}$ = 0.71073 Å) by using the APEX III software package.[18] Data for **Na-$PtPd_6$** were collected at 100 K on a Rigaku XtaLAB Synergy, Dualflex, HyPix single-crystal diffractometer equipped with kappa geometry (graphite monochromator, $\lambda_{Mo\ K\alpha}$ = 0.71073 Å) by using the CrysAlis^{Pro} software package.[19] The crystals were mounted in a Hampton cryoloop with paratone-N oil. Multi-scan absorption corrections were applied using the SADABS[20] and ABSPACK[21] program, respectively. The structures were solved by direct methods with the aid of successive difference Fourier maps, and were refined against all data using SHELXL-2014.[22] The H atoms of the cacodylate methyl groups were placed in calculated positions and refined using a riding model. All atoms were refined anisotropically, except for some oxygen atoms of crystal waters. Refinements were conducted by full-matrix least squares against |F| using all data. Images of the crystal structures were generated by Diamond, version 3.2 (software copyright, Crystal Impact GbR). Some of the lattice water molecules were too disordered and thus the disagreeable reflections were removed by the SQUEEZE command in PLATON.[23] Crystallographic data for **KNa-Pt_7** and **Na-$PtPd_6$** are summarized in Table 1. The cif files are provided free of charge by The Cambridge Crystallographic Data Centre (CCDC 2246656-2246657).

The catalytic reactions were carried out in a 100 mL Parr 5500 stainless-steel high-pressure compact reactor in conjunction with a Parr 4848 reactor controller and equipped with a magnetically coupled stirrer drive that ensured proper mixing of the reactants. In between the catalytic runs, the reactor was cleaned by washing with soap water thoroughly, rinsing with acetone and then drying at 100 °C in an oven. This was followed by gas chromatography (GC) analysis using a Shimadzu GC-2010 equipped with a flame ionization detector (FID) in order to measure the substrate conversion and selectivity of the obtained products via a HP-5 column (15 m × 0.25 mm, I.D. 0.25μm) with the carrier gas being He. The surface area of the supported catalysts was determined utilizing a gas adsorption analyzer. Nitrogen physisorption isotherms were measured at 77 K using a Quantachrome AUTOSORB 1 apparatus, and this was used to determine the Brunauer−Emmett−Teller (BET) surface area. The samples were degassed at 90 °C for 14 h. The specific surface areas were evaluated utilizing the BET method in the P/P_0 range of 0.05−0.35. The pore volumes were measured using the BJH analysis method.

Bond valence sum calculations. The bond valence sum (BVS) calculations were performed on a program copyrighted by Chris Hormillosa & Sean Healy and distributed by I. D. Brown.[24] In **KNa-Pt$_7$** and **Na-PtPd$_6$**, the BVS values for the central Pt atoms are 3.992 and 3.778, respectively. In **KNa-Pt$_7$**, the BVS values for the six surrounding Pt atoms range from 1.990 to 1.943. In **Na-PtPd$_6$**, the BVS values for the six surrounding Pd atoms range from 2.123 to 2.178. The BVS values for different types of μ_3-bridging oxygens are presented in Tables S1 and S2. These values show that these oxygens are not protonated and therefore the central Pt ion is in the 4+ oxidation state and the surrounding Pt and Pd ions are in the 2+ oxidation state, respectively.

KNa[Pt^{IV}Pt$^{II}_6$O$_6$(AsO$_2$(CH$_3$)$_2$)$_6$]·NaNO$_3$·NaAsO$_2$(CH$_3$)$_2$·21H$_2$O (KNa-Pt$_7$). $H_2Pt(OH)_6$ (9 mg, 0.03 mmol) was dissolved in 0.1 mL of 1 M NaOH. This solution was added to 2 mL of 2 M sodium dimethylarsinate buffer (pH 7) containing K_2PtCl_4 (75 mg, 0.18 mmol), and stirred for 1 h at 80 °C. After two weeks, red block-shaped crystals were collected by filtration and washed with 96% ethanol. Yield: 9 mg (10% with respect to $H_2Pt(OH)_6$ as limiting reagent). Elemental Analysis: Calculated (%) for **KNa-Pt$_7$**: Pt 46.00, As 17.67, K 1.32, Na 2.32, C 5.66, H 2.85, N 0.47. Found (%): Pt 46.00, As 18.40, K 1.38, Na 2.28, C 5.13, H 2.52, N 0.43. FT-IR (KBr/cm^{-1}): 3600-3300 (s) [ν(O-H) of H_2O], 3003-2922 (w) [ν(C-H) methyl groups of cacodylate], 1633 (m) [H_2O bending fundamental mode δ],

1383 (s) [δ(C-H) methyl groups of cacodylate], 1267 (m) [$\delta_{in\text{-}plane}$(O-H)], 1056 (w) [$\nu_{sym(N\text{-}O)}$ of NO_3^-], 898 (w) [$\delta_{out\text{-}of\text{-}plane}$(O-H)], 794-604 (s) [ν(Pt-O)], 505 (m) [ν(As-C)].

$Na_2[Pt^{IV}Pd^{II}_6O_6(AsO_2(CH_3)_2)_6]\cdot 2NaNO_3\cdot 9H_2O$ (Na-PtPd$_6$). $H_2Pt(OH)_6$ (9 mg, 0.03 mmol) was dissolved in 0.1 mL of 1 M NaOH. This solution was added to 2 mL of 2 M sodium dimethylarsinate buffer (pH 7) containing $Pd(NO_3)_2$ (43 mg, 0.18 mmol), and stirred for 1 h at 80 °C. After ten days, red needle-shaped crystals were collected by filtration and washed with 96% ethanol. Yield: 30 mg (47% with respect to $H_2Pt(OH)_6$ as limiting reagent). Elemental Analysis: Calculated (%) for **Na-PtPd$_6$**: Pt 9.16, Pd 29.98, As 21.11, Na 4.32, C 6.77, H 2.56, N 1.32. Found (%): Pt 8.90, Pd 29.80, As 21.70, Na 4.11, C 7.13, H 2.28, N 1.01. FT-IR (KBr/cm^{-1}): 3600-3300 (s) [ν(O-H) of H_2O], 3007-2853 (w) [ν(C-H) of methyl groups of cacodylate], 1639 (m) [H_2O bending fundamental mode δ], 1384 (s) [δ(C-H) of the methyl groups of cacodylate], 1268 (m) [$\delta_{in\text{-}plane}$ (O-H)], 1050 (w) [$\nu_{sym(N\text{-}O)}$ of NO_3^-], 904 (w) [$\delta_{out\text{-}of\text{-}plane}$ (O-H)], 806-581 (s) [ν(Pt-O), ν(Pd-O)], 514-491 (m) [ν(As-C)].

SBA15 and **SBA15-apts**. A modified synthetic procedure was used to synthesize SBA15 (Santa Barbara Amorphous-15).[25] In a typical synthesis, 120.0 g of Pluronic® P123 (Mn ~ 5,800, Sigma Aldrich) was stirred in a mixture of 100 mL of 37% HCl and 3.6 L of water until complete dissolution (~ 4 hours). To this solution, 270 mL of TEOS was added dropwise and stirred in a water bath for 16 hours at 36 ºC. Subsequently, the solution was aged at 95 ºC under static conditions for 3 days. The resulting white precipitate was collected by filtration, dried in air for 2 days followed by calcination at 550 ºC for 6 hours under air with a heating rate of 1 ºC/min in order to remove the template. Following this, a mixture of (3-aminopropyl)triethoxysilane (18 mL) and SBA15 (33.0 g) was refluxed for 5 hours in 1 litre of toluene followed by filtration at room temperature. The resultant white powder was dried at 100 ºC for 5 hours to obtain the SBA15-apts.

KNa-Pt$_7$@SBA15-apts. The **KNa-Pt$_7$** (20 mg, 0.0067 mmol) was dissolved in 100 mL of deionized water followed by the slow addition of 380 mg of the SBA15-apts to the resulting orange coloured solution under stirring. The quantities of the **KNa-Pt$_7$** and support were taken such that the resultant composite material would have a ~5 wt% Pt-loading. After refluxing for 2 h, the mixture was filtered under vacuum and the residue was washed three times with deionized water and air-dried. The filtrate was found to be colourless, which indicated quantitative loading. The dried **KNa-Pt$_7$@SBA15-apts**

composite material was then calcined at 250 ºC for 4 h (heating rate = 0.5 ºC/min) in order to obtain the calcined pre-catalyst that was eventually reduced in situ under H_2 inside the Parr compact reactor to generate the catalyst for the hydrogenation of arenes.

Catalytic Hydrogenation. In a typical catalytic reaction, 50 mg of the catalyst (0.005 mmol Pt content) was introduced into a 100 mL stainless-steel high-pressure Parr Compact reactor and 50 mL of a 0.5 M solution of the monocyclic arenes in n-hexane was added. The catalyst was then reduced *in situ* under H_2 (~50 bar) at 250 ºC and stirred for 1 min. Subsequently the reaction was started by increasing the temperature to 300 ºC and stirring the reaction mixture at 1000 rpm keeping the initial H_2 pressure at ~90 bar. Instead of using milder H_2 pressures, a high reaction pressure of ~90 bar was used in order to drive the reaction forward using the Le Châtelier's principle. The progress of the reaction was followed by monitoring the consumption of H_2 (pressure decrease) and gas chromatography (GC) analysis and the completion of the reaction was correlated with no further decrease in the H_2 pressures. Recyclability experiments on the catalyst were performed by filtering off and drying the used catalyst and utilizing it again in subsequent catalytic cycles under the same reaction conditions.

RESULTS AND DISCUSSION

Synthesis and Structure. We have discovered the first discrete mixed-valent polyoxoplatinate(IV,II), $[Pt^{IV}Pt^{II}_6O_6(AsO_2(CH_3)_2)_6]^{2-}$ (**Pt_7**) and the first platinum(IV)-centered polyoxopalladate(II) $[Pt^{IV}Pd^{II}_6O_6(AsO_2(CH_3)_2)_6]^{2-}$ (**$PtPd_6$**). Single-crystal XRD studies revealed that **Pt_7** crystallizes as a mixed potassium-sodium salt, $KNa[Pt^{IV}Pt^{II}_6O_6(AsO_2(CH_3)_2)_6]\cdot NaNO_3\cdot NaAsO_2(CH_3)_2\cdot 21H_2O$ (**KNa-Pt_7**), in the orthorhombic space group Pcca and **$PtPd_6$** crystallizes as a sodium salt, $Na_2[Pt^{IV}Pd^{II}_6O_6(AsO_2(CH_3)_2)_6]\cdot 2NaNO_3\cdot 9H_2O$ (**Na-$PtPd_6$**), in the triclinic space group P1, respectively. Both novel polyanions **Pt_7** and **$PtPd_6$** are isostructural, displaying a central distorted $Pt^{IV}O_6$ octahedron surrounded by a ring of six square-planar MO_4 (M = Pt^{II}, Pd^{II}) units with six terminal dimethylarsinate (also known as cacodylate, cac) ligands, resulting in a disk-shaped structure with idealized D_{3d} symmetry (Figure 1). Close inspection of the Pd7 and PtPd6 structures exhibit subtle differences in the bonding characteristics of the six cacodylate capping groups, rendering PtPd6 chiral (consistent with crystallization in the space group P1). This phenomenon could be rationalized by computational studies (see Supporting Information). All seven metal centers in both polyanions are coplanar forming a regular Pt^{IV}-centered M_6 hexagon (M = Pt^{II}, Pd^{II}) with metal-metal distances $Pt^{II}\cdots Pt^{II}$ 3.065-3.129 Å and $Pt^{IV}\cdots Pt^{II}$ 3.083-3.094 Å in **Pt_7** and $Pd^{II}\cdots Pd^{II}$ 3.009-3.102 Å and $Pt^{IV}\cdots Pd^{II}$ 3.038-3.076 Å in **$PtPd_6$**, respectively. The octahedral coordination environment of the central Pt^{IV} ions is formed exclusively by μ_3-oxo

groups and the Pt^{IV}–O bond distances are in the range of 2.023–2.033 Å in **Pt_7**, and in the range of 2.037–2.071 Å in **$PtPd_6$**. The square-planar coordination environments of the Pt^{II} and Pd^{II} ions in **Pt_7** and **$PtPd_6$**, respectively, are formed by two μ_3-oxo groups and two cacodylate oxygens (Pt^{II}–O: 1.998–2.071 Å; Pd^{II}–O: 1.964–2.064 Å). The average Pt^{IV}–O bond length in **Pt_7** of 2.029 Å and in **$PtPd_6$** of 2.023 Å is comparable with that of 2.01 Å observed in $[H_3PtW_6O_{24}]^{5-}$.[10a] Bond valence sum (BVS) calculations suggest no protonation for any of the oxygen atoms in **Pt_7** and **$PtPd_6$** (Tables S1 and S2).

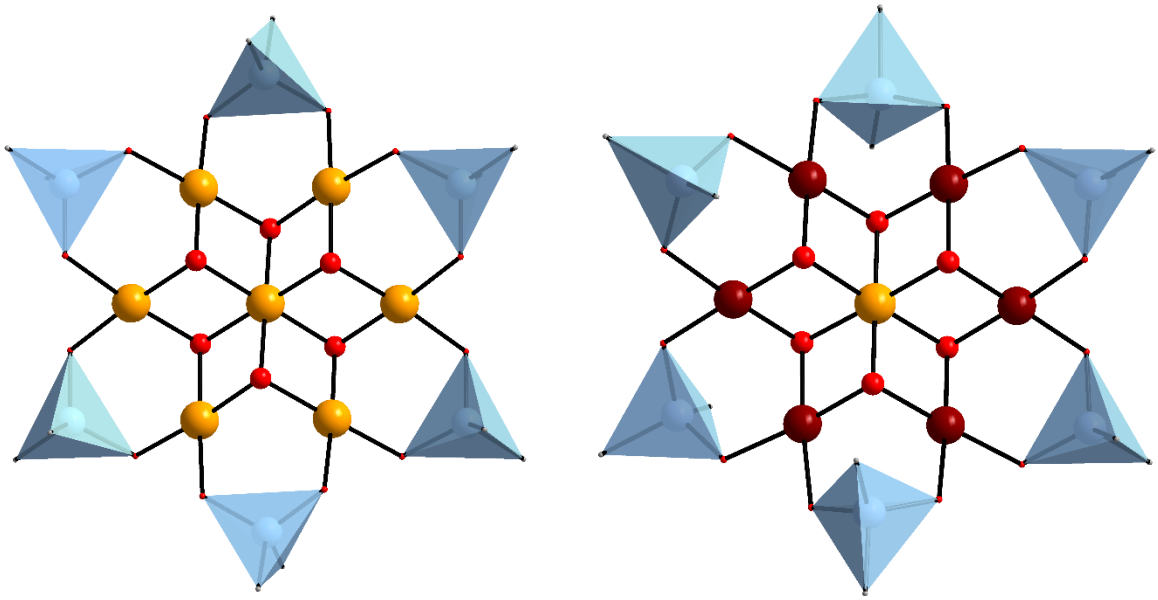

Figure 1. Structural representation of **Pt_7** (left) and **$PtPd_6$** (right). Color code: Pt (orange), Pd (dark red), O (red), C (gray), $\{(CH_3)_2AsO_2\}$ (blue tetrahedra); hydrogens omitted for clarity.

Table 1. Single crystal data and structure refinement parameters for **KNa-Pt_7** and **Na-$PtPd_6$**.

Compound	**KNa-Pt_7**	**Na-$PtPd_6$**
empirical formula[a]	$KNa_3Pt_7As_7C_{14}H_{84}O_{44}N$	$Na_4PtPd_6As_6C_{12}H_{54}O_{33}N_2$
fw,[a] g mol^{-1}	2968.86	2129.64
crystal system	Orthorhombic	Triclinic
space group	*P*cca	*P*1
a(Å)	26.8981(9)	6.71005(9)

b(Å)	13.4671(4)	15.14730(18)
c(Å)	19.6627(7)	15.2445(2)
α(°)	90	62.3352(13)
β(°)	90	86.3984(12)
γ(°)	90	88.6937(11)
V (Å^3)	7122.6(4)	1369.56(3)
Z	4	1
Dc (g cm^{-3})	2.499	2.532
abs coeff, mm^{-1}	16.603	8.171
F(000)	4768	971
θ range for data collection, deg	2.206 to 26.477	2.680 to 25.027
completeness to Θ_{max}	99.8 %	99.9%
index ranges	-33 =< h =< 33, -16 =< k =< 16, -22 =< l =< 24	-7 =< h =< 7, -18 =< k =< 18, -18 =< l =< 18
reflns collected	56395	91736
indep reflns	7294	9526
R(int)	0.1190	0.0851
abs corn	Semi-empirical from equivalents	Semi-empirical from equivalents
data/restaints/param	7294/18/302	9526 / 3 / 575
GOF on F^2	1.020	1.046
R_1,[b] wR_2[c] [I >2σ(I)]	0.0465, 0.1188	0.0339, 0.0922
R_1,[b] wR_2[c] (all data)	0.0860, 0.1356	0.0353, 0.0934
Absolute structure parameter	/	0.479(6)
Largest diff peak and hole, e Å^{-3}	1.533 and -2.517	3.133 and -2.588

[a]The entries are the actual formula units and weights as obtained from bulk elemental analysis.
[b]$R_1 = \Sigma||F_o| - |F_c||/\Sigma|F_o|$. [c]$wR_2 = [\Sigma w(F_o^2 - F_c^2)^2/\Sigma w(F_o^2)^2]^{1/2}$.

Mass Spectroscopy. ESI-mass spectra of **KNa-Pt$_7$** and **Na-PtPd$_6$** were acquired from aqueous solutions in the negative ion mode. For **Pt$_7$**, two groups of signals centered around *m*/*z* 1141 and 2284 were observed (Figure 2). As a starting point for spectra assignment, we assumed the presence of the core structure $[Pt^{IV}Pt^{II}_6O_6(AsO_2(CH_3)_2)_6]^{2-}$ (**Pt$_7$**) as established by XRD, and the observed isotope pattern is in full agreement with this structure. The signal centered around *m*/*z* 1141 can be assigned to a doubly-charged species based on the spacing of the isotope peaks (Figure 2). The simulated mass

spectrum is in good agreement with the experimentally observed spectrum. The signal centered at around *m/z* 2284 can be assigned to a singly-charged ion accompanied by a proton, suggesting that the charge of the oxo-cluster is reduced from 2- to 1- (Figure 2). For the structural analogue **PtPd$_6$**, one signal was observed in the negative ion mode centered at *m/z* 875 with isotope patterns expected for the structure (Figure 3). Following spectral simulations, we assigned these signals to the doubly-charged species $[Pt^{IV}Pd^{II}_6O_6(AsO_2(CH_3)_2)_6]^{2-}$ (**PtPd$_6$**) (Figure 3).

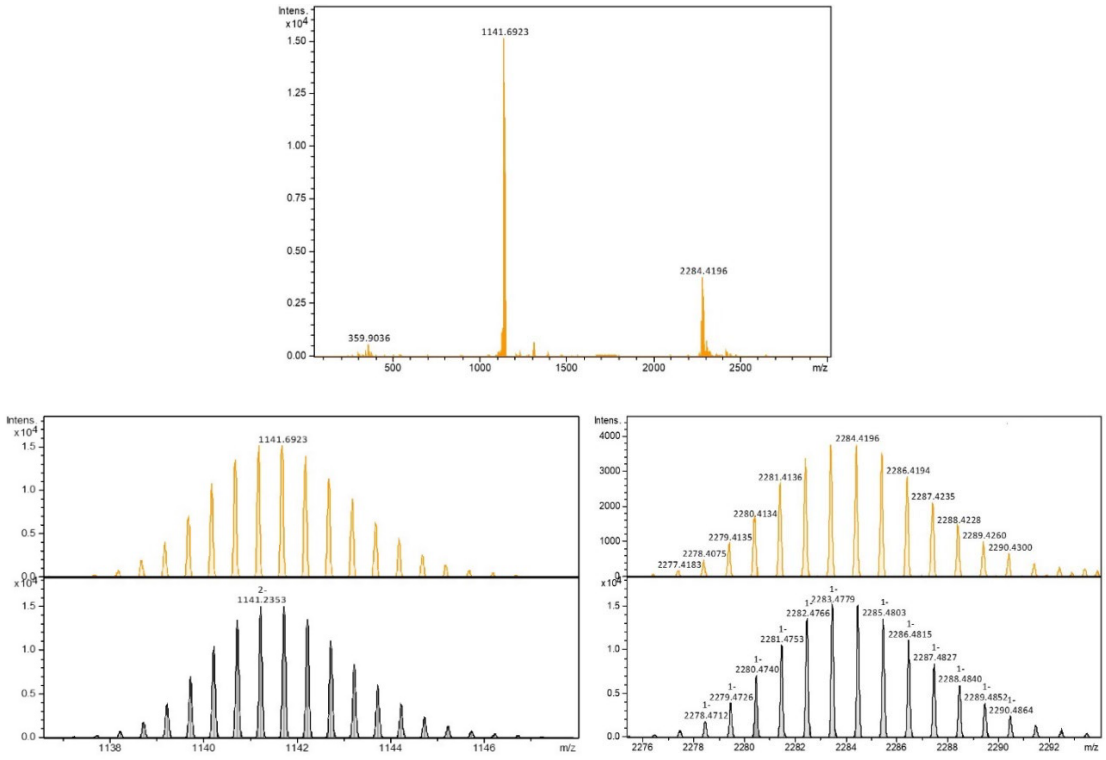

Figure 2. Top: ESI-MS spectrum (full scan) of an aqueous solution of **KNa-Pt$_7$** in the negative-ion mode; Bottom left: Simulated (bottom panel) and experimental ESI-MS spectrum (top panel) of a doubly charged $[Pt_7O_6((CH_3)_2AsO_2)_6]^{2-}$ ion (expanded view); Bottom right: Simulated (bottom panel) and experimental ESI-MS spectrum (top panel) of a singly charged $[HPt_7O_6((CH_3)_2AsO_2)_6]^{-}$ ion (expanded view).

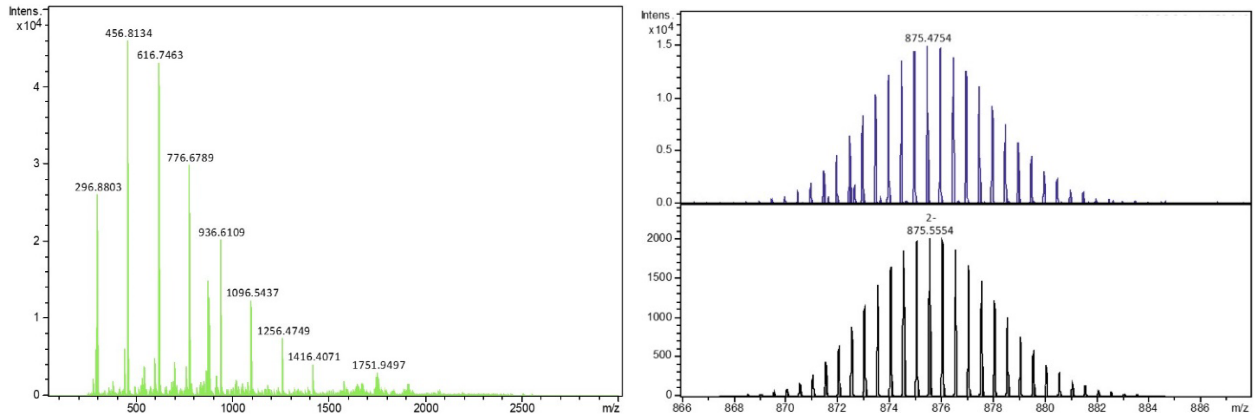

Figure 3. Left: ESI-MS spectrum (full scan) of an aqueous solution of **Na-PtPd$_6$** in the negative-ion mode; Right: Simulated (bottom panel) and experimental ESI-MS spectrum (top panel) of a doubly charged $[PtPd_6O_6((CH_3)_2AsO_2)_6]^{2-}$ ion (expanded view).

XPS Spectroscopy. X-ray photoelectron spectroscopy (XPS) measurements were performed on both **KNa-Pt$_7$** and **Na-PtPd$_6$** in order to ascertain the oxidation states of Pt and Pd. Both **Pt$_7$** and **PtPd$_6$** exhibited a Pt 4f$_{7/2}$ band at ~74.9 eV, which is typical for Pt in the 4+ oxidation state. The XPS spectrum of **Pt$_7$** exhibited characteristic 4f$_{7/2}$ peaks at ~72.5 eV and ~74.9 eV with a ratio of 6 :1, indicating that Pt is present in the 2+ and 4+ oxidation states, respectively (Figure 4). The XPS spectrum of **PtPd$_6$** exhibited the characteristic Pd 3d$_{5/2}$ band at 337.2 eV, which is typical for Pd in the 2+ oxidation state (Figure 5). These observations were also corroborated by bond valence sum (BVS) calculations on Pt and Pd in **Pt$_7$** and **PtPd$_6$**, which indicated that the central Pt ion is in the 4+ oxidation state and the surrounding Pt and Pd ions are in the 2+ oxidation state.

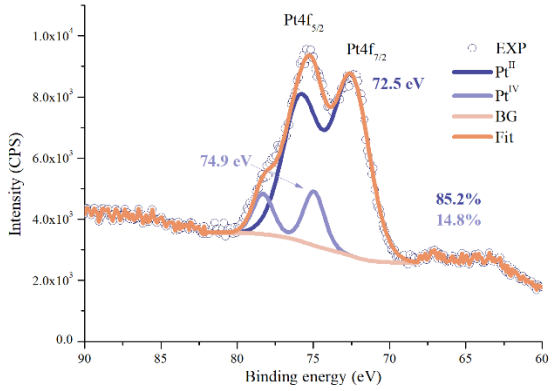

Figure 4. X-ray photoelectron spectra and fits for Pt 4f$_{7/2}$ and 4f$_{5/2}$ doublet of **KNa-Pt$_7$**.

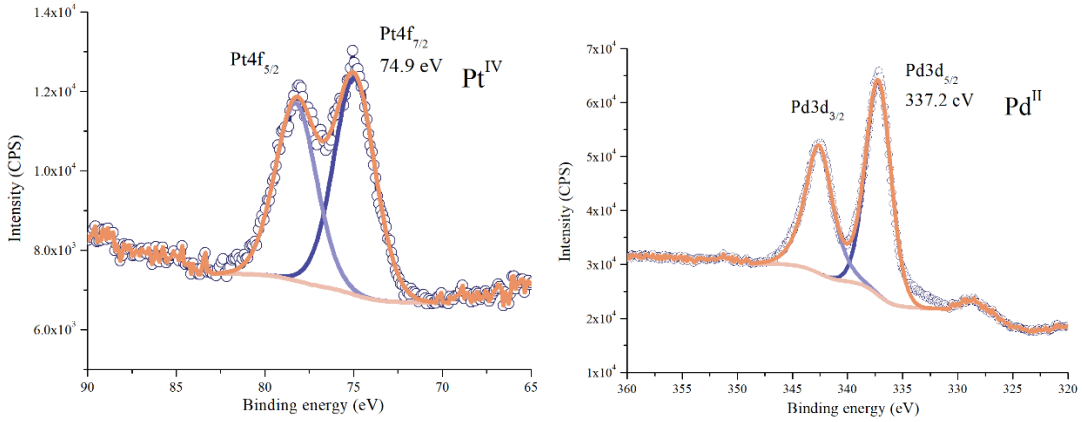

Figure 5. X-ray photoelectron spectra and fits for Pt $4f_{7/2}$ and $4f_{5/2}$ doublet of **Na-PtPd$_6$** left), and Pd $3d_{5/2}$ and $3d_{3/2}$ doublet of **Na-PtPd$_6$** (right).

Solution NMR Spectroscopy. To complement our solid-state XRD results on **Pt$_7$** and **PtPd$_6$** with solution studies, we performed ^{1}H, ^{13}C and ^{195}Pt NMR measurements on **KNa-Pt$_7$** and **Na-PtPd$_6$** redissolved in H_2O/D_2O. The ^{1}H (D_2O) NMR spectrum of sodium cacodylate (Na-cac) exhibits sharp peaks at 4.70 and 1.41 ppm, respectively, corresponding to the protons of the crystal water molecules and cacodylate methyl groups, respectively. The ^{1}H (D_2O) NMR spectra of **Pt$_7$** and **PtPd$_6$** exhibit theexpected two peaks at 2.36 and 1.60 ppm for **Pt$_7$** and 2.38 and 1.60 ppm for **PtPd$_6$**, respectively, corresponding to the two structurally and hence magnetically inequivalent cacodylate methyl groups (Figure 6). The small peak at 1.64 ppm for **Pt$_7$** corresponds to the methyl groups of co-crystallized cacodylate (Figure S3). On the other hand, the small peak at 1.62 ppm for **PtPd$_6$** can be assigned to free cacodylate, which is formed *in situ* by partial decomposition of **PtPd$_6$**. This observation is further supported by the time-dependent ^{1}H spectrum of **PtPd$_6$** (Figure 7). The ^{1}H NMR spectrum of **Pt$_7$** remained unchanged even for two months, which indicates the high solution stability of this polyanion (Figure S4). The ^{13}C (D_2O) NMR spectrum of Na-cac exhibits a narrow peak at 17.4 ppm, whereas the ^{13}C (D_2O) NMR spectrum of **Pt$_7$** exhibits peaks at 18.7 and 15.7 ppm, corresponding to the two crystallographically inequivalent cacodylate methyl groups (Figure 6). For **PtPd$_6$**, the expected two signals were observed with chemical shift values of 20.3 and 16.7 ppm, respectively. In analogy to the ^{1}H NMR spectrum, there is also a small peak at 17.3 ppm for this compound. The ^{195}Pt spectrum of **Pt$_7$** shows a broad singlet at 727 ppm (Figure 8), which is assigned to Pt^{II}. On the other hand, we could not observe any signal for the Pt^{IV} center. However, the ^{195}Pt NMR spectrum of **PtPd$_6$** revealed the expected singlet at 4080 ppm, which is unequivocally due to the central Pt^{IV} ion (Figure 8). The

chemical shift of ^{195}Pt NMR of polyainons **Pt$_7$** and **PtPd$_6$** were confirmed by DFT calculations (*vide infra*). In any case, the combination of ^{1}H and ^{13}C NMR spectra is fully consistent with the solid-state structures of **Pt$_7$** and **PtPd$_6$**, providing clear evidence for the presence of the polyanion in solution.

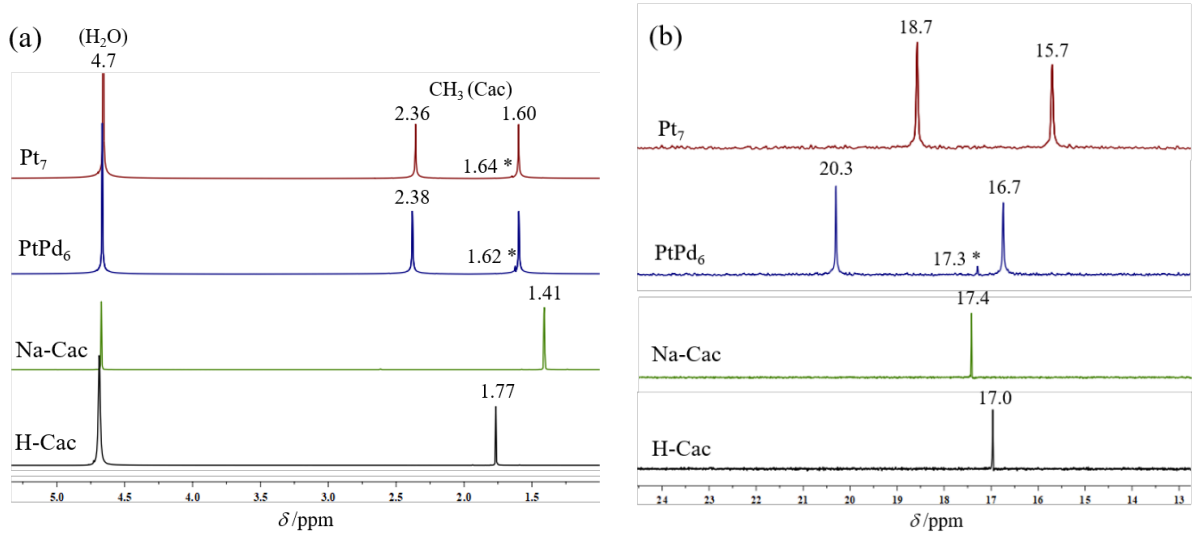

Figure 6. ^{1}H (a) and ^{13}C (b) NMR spectra (D_2O) of **Pt$_7$** and **PtPd$_6$** compared to spectra of the references cacodylic acid (H-cac) and sodium cacodylate (Na-cac). The * represents free cacodylate ions.

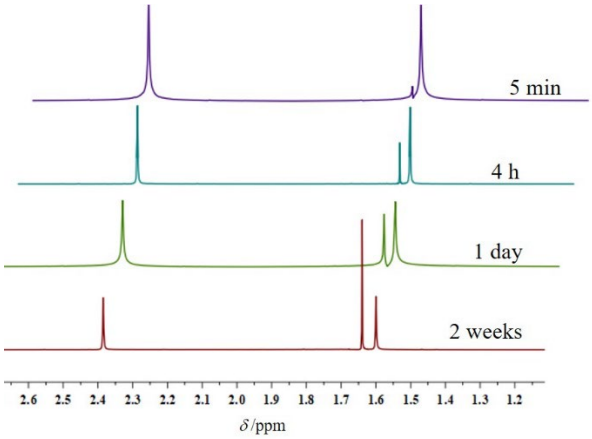

Figure 7. Time dependent ^{1}H spectra (D_2O) of **Na-PtPd$_6$**.

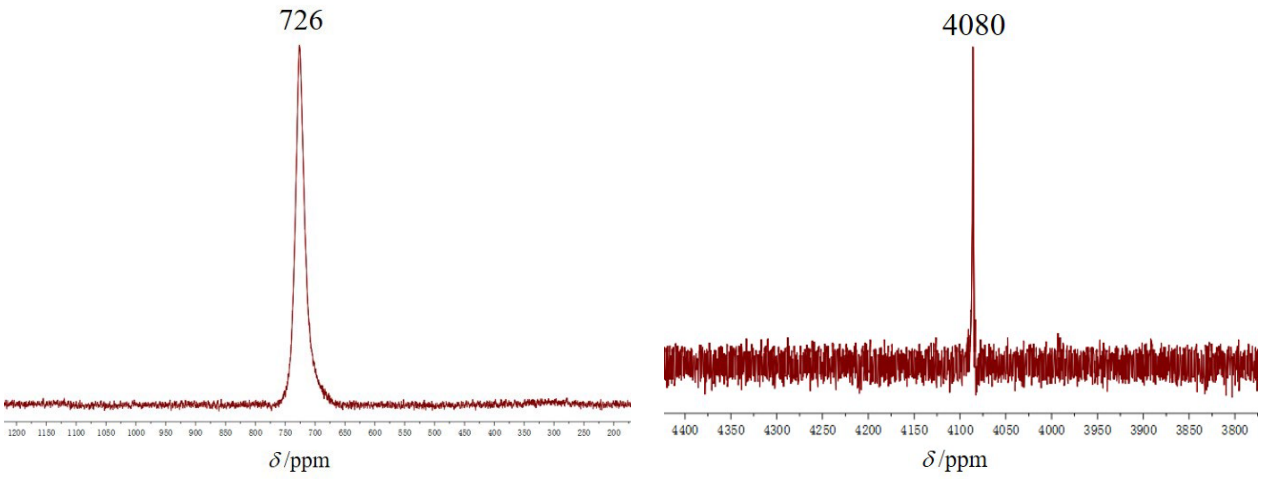

Figure 8. ^{195}Pt NMR spectra of **KNa-Pt$_7$** (left) and **Na-PtPd$_6$** (right) redissolved in water.

Computational Studies. The structures of the anions **Pt$_7$** and **PtPd$_6$** have been computationally optimized using Density Functional Theory (DFT) methods (B3LYP[26] and OPBE[27]) together with the basis sets 6-31g(d,p)[28] for light atoms (H, O and C) and LANL2DZ[29] with corresponding Effective Core Potentials for the heavier elements (Pt, Pd and As), the aqueous environment has been simulated through a continuum model, namely PCM,[30] as implemented in Gaussian.[31] The geometries obtained for **Pt$_7$** where compared with the available crystal structures, a root-mean-square deviation (RMSD) of 0.24 and 0.22 Å (without hydrogens) was found respectively using B3LYP and OPBE functionals, indicating that both functionals provide geometries similar to the crystal structures (note calculations are in aqueous solution). To simulate the ^{195}Pt NMR spectra of these two anions, ADF[32] calculations with different functionals together with the TZ2P[33] basis set, relativistic spin-orbit ZORA,[34] simulation of the water environment with COSMO[35] and Gaussian nuclear distribution model[36] were run on the previously optimized structures, and the selected results are presented in Table 2. Computationally derived NMR chemical shifts (δ_{cal}) are strongly dependent on the methodology used.[37,4b,5c] For **Pt$_7$** and **PtPd$_6$** the best results compared to experiment were achieved using SSB-D[38] and OPBE methods on B3LYP geometries, similarly to previously reported results[4b] on similar systems. Predicted NMR shifts show errors from few ppm to few hundreds of ppm. However, the difference on the NMR chemical shifts of Pt^{IV} in **PtPd$_6$** and the average of the six Pt^{II} in **Pt$_7$** shows only a small error. This difference of the two signals is 3408 ppm with SSB-D and 3548 ppm with OPBE, which are both close to the experimentally measured difference of 3354 ppm. This suggests that the predicted signal for Pt^{IV} in **Pt$_7$** should appear in the range above 4080 and below 4500 ppm, whereas the Pt^{II} signals in this type

of complex should appear around 700 ppm. It can be concluded that the assignments of the experimental ^{195}Pt NMR chemical shifts described in this work are correct.

Table 2. Computationally predicted NMR chemical shifts (δ_{calc}) in ppm for **Pt$_7$** and **PtPd$_6$** using different methods.[a]

Compound	**PtPd$_6$**	**Pt$_7$**		
Metal center	Pt^{IV}	Pt^{II}	Pt^{IV}	**Pt^{IV} - Pt^{II}** [b]
SSB-D/B3LYP[c]	3854	446	4057	3408
SSB-D/OPBE[c]	4415	802	4696	3613
OPBE/B3LYP[c]	4307	759	4538	3548
BP86/B3LYP[c]	4503	895	4628	3763
Experimental	*4080*	*726*	---	*3354*

[a] All chemical shifts δ_{calc} (in ppm) correspond to differences between the predicted ^{195}Pt NMR shielding for indicated species and NMR shielding of ^{195}Pt NMR reference $PtCl_6^{2-}$ both at the same level of theory.
[b] Difference between the averaged signal of the unique Pt^{IV} in the **PtPd$_6$** anion and the signal of the six Pt^{II} nuclei in the **Pt$_7$** anion.
[c] Notation Method1/Method2 corresponds to: Method 1 is the method used for NMR calculations in ADF, Method 2 is the method used for geometry optimization in Gaussian.

Catalytic Studies. The hydrogenation of arenes provides a direct and retrosynthetically simple route towards saturated carbo- and heterocycles. This is an important industrial process with a wide range of applications ranging from the production of functional materials, important intermediates in organic synthesis, pharmaceuticals, to the improvement of diesel fuel quality.[39] Metals, especially noble metals and their nanoparticles, have been found to be highly effective catalysts in this area. The reduction of noble metal salts and the decomposition/reduction of organometallic compounds are both common methods for forming noble metal nanoparticles.[40] In both cases, the resulting nanoparticles are typically stabilized by ligands or capping groups such as polymers, dendrimers, ionic liquids, and surfactants, in order to prevent uncontrolled aggregation. Recently, the anionic template-assisted method was used to synthesize a series of silver nanocrystals (NCs) with different sizes and shapes.[41] However, these methods do not allow for an elegant control over the size and shape of the resulting nanoparticles. Therefore, our aim has been to design and synthesize discrete noble metal-based oxo clusters having a particular size, shape, and nuclearity, and subsequently loading them onto stable and catalytically inert supports with high surface area, such as SBA15. Subsequent thermal reduction under

a H_2 atmosphere would then yield SBA15 supported nanoparticles of controlled sizes and shapes, which would depend on the size and shape of the parent noble metal-oxo clusters.

Thus, we have investigated the efficacy of the porous silica-supported **Pt_7** as a heterogeneous precatalyst in the hydrogenation of *o*-xylene. The *o*-xylene was chosen as a model substrate to study the efficacy of the **Pt_7@SBA15-apts** catalyst because the reaction rate for *o*-xylene was the slowest among the monocyclic arenes (*p*-xylene > *m*-xylene > *o*-xylene).[42] For the catalytic studies, **KNa-Pt_7** was used as the precursor, and the supported precatalyst **Pt_7@SBA15-apts** was obtained by dissolving **KNa-Pt_7** in water and slowly adding the 3-aminopropyltriethoxysilane (apts)-modified SBA15 (SBA15-apts) to the stirred solution, which was subsequently refluxed for 2 h (Pt loading ≈ 5 wt %. The mixture was filtered, and the residue was washed multiple times with deionized water, air-dried, and subsequently calcined at 250 ºC for 4 h (heating rate = 0.5 ºC/min) in order to obtain the precatalyst **Pt_7@SBA15-apts** that was eventually reduced *in situ* under H_2 inside the Parr reactor, thereby generating the actual catalyst for the hydrogenation of arenes. It was found that for *o*-xylene as the substrate, the reaction was complete in ~10 min with a ~96% conversion and a *cis*/*trans* ratio ($S_{c/t}$) of 67:29, which is opposite of the selectivity of the *trans*-1,2-DMCH favored with Pd-based catalysts (Table 3). The reaction of arenes with SBA15-apts alone did not show any hydrogenation activity. The catalyst was also found to be recyclable up to 3 consecutive reaction cycles with a slightly increase in the reaction conversion (Table 3). Also, N_2 sorption measurements were performed on the precatalyst before and after loading/calcination and after catalysis, provided valuable insights into the effect of these processes on the surface area of the material (Figure 9, Table S3). It was observed that the surface area as well as the pore volume of the unmodified SBA15 support (434 m^2/g and 0.691 cc/g) decrease after modification with apts (377 m^2/g and 0.535 cc/g), as expected. Immobilization of **KNa-Pt_7** on the modified SBA15 further decreases the surface area and pore volume, which indicates that the pores are partially blocked upon loading, as expected. These values increase again upon calcination due to loss of the aminopropyl arms from the silica surface. After catalysis, there is a subsequent decrease in the surface area and pore volume, probably due to partial blocking of the pores by the Pt nanoparticles. The ^{1}H NMR spectrum of the filtrate obtained after loading the **KNa-Pt_7** on the modified SBA15 support only exhibited one peak at 4.7 ppm, corresponding to water, confirming that during the loading process the **Pt_7** polyanion has been adsorbed quatitatively into the pores of the SBA-15 (Figure S5).

The activity of **KNa-Pt$_7$** as a heterogeneous hydrogenation precatalyst has been compared with the other Pt-based catalysts, and various polyoxopalladates (POPds) supported on SBA15-apts (Table 3). **Pt$_7$@SBA15-apts** has the distinct advantage of requiring a much lower activation temperature with excellent activity and recyclability.

Table 3. *o*-xylene hydrogenation at 300 °C and 90 bar H_2 pressure using different supported catalyst materials (support = SBA15-apts).

Pre-Catalyst	**M loading (mmol)**	**Activation Method**	**Reaction Time (min)**	**Conversion (%)**	**Selectivity ($S_{c/t}$)**	**References**
KNa-Pt$_7$	0.005	250 ºC air calcination (4 h)	10	~96 (1st cycle) ~99 (2nd cycle) ~100 (3rd cycle)	$S_{c/t}$ = 67/29 $S_{c/t}$ = 66/33 $S_{c/t}$ = 65/35	This work
Pd_{40}-SiW_{12}	0.009	250 ºC air calcination (4 h)	55	~99	37/63	6b
$Pd_{13}As_8$	0.01	Chemical reduction by hydrazine, 650 ºC air calcination (4.5 h)	960	~100	40/60	43
$Pd_{13}Se_8$	0.01	550 ºC air calcination (4.5 h)	50	~100	43/57	
$NiPd_{12}Se_8$	0.01	550 ºC air calcination (4.5 h)	25	~100	40/60	
$Pd_{15.4}P_{10}$	0.01	550 ºC air calcination (4.5 h)	15	~100	40/60	
$Na_{10}[Pt_3S_2(SO_3)_6]$	0.006	425 ºC air calcination (1 h)	150	~100 (150 ºC) ~100 (350 ºC)	70/30 75/25	4b
Pt/Al_2O_3	0.002	500 ºC air calcination (12 h)	180	27.4 (250 ºC)	——	44
Silicalite-1@Pt/α-Al_2O_3	0.1	500 ºC air calcination (4 h)	240	80.7 (200 ºC)	——	45
Pt/C_{12}MCM-41	0.013	300 ºC H_2 reduction (2 h)	120	38 (110 ºC)	25/13	46

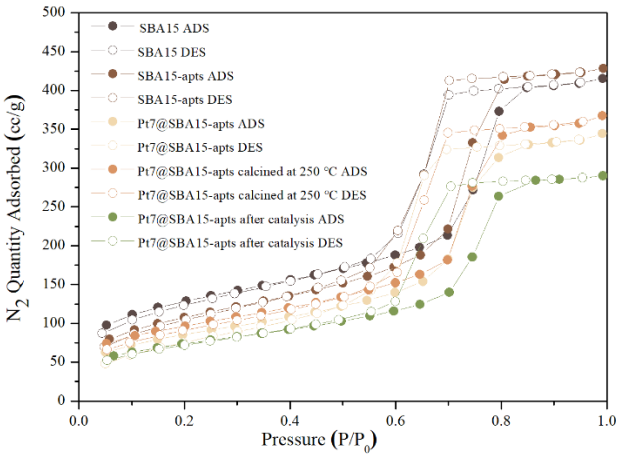

Figure 9. N_2 sorption isotherms of the SBA15 support before and after modification, after immobilization with **KNa-Pt$_7$** and after calcination and catalysis.

As mentioned above, for **Pt$_7$** a higher selectivity towards the formation of the *cis*-isomer was observed. On the other hand, when using polyoxopalladate (POPd) based catalysts a higher selectivity for the formation of the *trans*-isomer was observed,[43] and this is in line with results reported for *o*-xylene hydrogenation over supported Pd, Ni and Pt catalysts.[47] The nature of the catalyst and the operation conditions have a strong effect on the product stereoselectivity, such as temperature and metal dispersion.[48] The *o*-xylene substrate is believed to adsorb parallel to the metal surface because of the interaction between the π-electrons in the aromatic ring and the empty *d*-metal orbitals.[49] To reduce the repulsive effect, the two methyl substituents in *o*-xylene should be oriented away from the surface, and consequently *cis*-DMCH should be obtained predominantly. Hence, the *cis* stereoisomer is the kinetically favored product, whereas the *trans* stereoisomer is thermodynamically favored.[47a] The increased selectivity of the *trans*-isomer as a function of temperature and increased metal dispersion has been rationalized by a roll-over mechanism proposed by Inuone,[50] where the model explains well the exchange of hydrogen atoms on both sides of a cyclopentane molecule (over Pd catalysts). Therefore, the *cis*/*trans* ratio of the final product is opposite for Pt- and Pd-based catalysts.

CONCLUSIONS

In summary, we have synthesized and structurally characterized the first mixed-valent polyoxo-platinate(IV,II) **Pt$_7$** and the first Pt^{IV}-containing polyoxopalladate(II) **PtPd$_6$** as discrete inorganic oxo

complexes by using simple open beaker and aqueous solution synthetic conditions. Both polyanions **Pt_7** and **$PtPd_6$** were fully characterized in the solid state and the oxidation states of the noble metal ions were unequivocally identified. The solution (^{1}H, ^{13}C and ^{195}Pt NMR) and gas phase studies also support the existence of the two polyanions. In fact, **Pt_7** was shown to be stable in solution for several months, which provides much potential for further studies and applications, e.g. in the catalytic or biomedical directions. We have also shown that the **Pt_7** polyanion supported on porous silica can be an effective heterogeneous catalyst for the hydrogenation of arenes. Our work can be considered as a synthetic breakthrough in polyoxoplatinate (POPt) and platinum-containing polyoxopalladate (POPd) chemistry, and besides performing catalytic studies (e.g. hydrogenation of olefins using the novel polyanions homogeneously or as bottom up precursors for supported noble metal nanoparticles) we aim at the synthesis of more derivatives of this family of polyoxo-noble-metalates in the future.

ASSOCIATED CONTENT

Supporting Information

The Supporting Information is available free of charge at xxxxx.

Surface area measurements of catalyst, additional single-crystal structural figures, TGA and IR plots, additional NMR spectra.

Accession Codes

CCDC 2246656-2246657 contain the supplementary crystallographic data for this paper. These data can be obtained free of charge via www.ccdc.cam.ac.uk/structures/, or by emailing data_request@ccdc.cam.ac.uk, or by contacting The Cambridge Crystallographic Data Centre, 12 Union Road, Cambridge CB2 1EZ, UK; fax: +44 1223 336033.

AUTHOR INFORMATION

Corresponding Author

Ulrich Kortz − School of Science, Constructor University, Campus Ring 1, 28759 Bremen, Germany; orcid.org/0000-0002-5472-3058; Email: ukortz@constructor.university, u.kortz@jacobs-university.de

Authors

Jiayao Zhang − School of Science, Constructor University, Campus Ring 1, 28759 Bremen, Germany; orcid.org/0000-0003-2131-4298

Saurav Bhattacharya – School of Science, Constructor University, Campus Ring 1, 28759 Bremen, Germany and Department of Chemistry, BITS Pilani K. K. Birla Goa Campus, 403726 Goa, India; orcid.org/0000-0002-3396-8312

Bahaa E. Khsara − School of Science, Constructor University, Campus Ring 1, 28759 Bremen, Germany

Talha Nisar − School of Science, Constructor University, Campus Ring 1, 28759 Bremen, Germany; orcid.org/0000-0003-0091-362X

Anja B. Müller − School of Science, Constructor University, Campus Ring 1, 28759 Bremen, Germany

Maria Besora − Departament de Química Física i Inorgànica, Universitat Rovira i Virgili, 43007 Tarragona, Spain; orcid.org/0000-0002-6656-5827

Josep M. Poblet − Departament de Química Física i Inorgànica, Universitat Rovira i Virgili, 43007 Tarragona, Spain; orcid.org/0000-0002-4533-0623

Veit Wagner − School of Science, Constructor University, Campus Ring 1, 28759 Bremen, Germany; orcid.org/0000-0002-6831-8600

Nikolai Kuhnert − School of Science, Constructor University, Campus Ring 1, 28759 Bremen, Germany; orcid.org/0000-0003-1681-8424

Complete contact information is available at:

Notes

The authors declare no competing financial interest.

ACKNOWLEDGMENTS

U. K. thanks the German Research Council (DFG, KO-2288/26-1) and Constructor University for support. J. Z. sincerely acknowledges CSC (China Scholarship Council) for a doctoral fellowship.

Keywords: Platinum • Palladium • Polyoxometalate • ESI-MS • XPS • ^{195}Pt NMR

REFERENCES

(1) (a) Pope, M. T., *Heteropoly and Isopoly Oxometalates*, Springer-Verlag, Berlin Heidelberg, 1983; (b) Pope, M. T.; Müller, A., Polyoxometalate Chemistry: An Old Field with New Dimensions in Several Disciplines. *Angew. Chem. Int. Ed.* **1991**, *30*, 34-48.

(2) (a) Pope, M. T.; Müller, A., *Polyoxometalate Chemistry: From Topology via Self-Assembly to Applications*, Kluwer Academic Publishers: Dordrecht, Netherlands, 2001; (b) Wang, S. S.; Yang, G. Y., Recent Advances in Polyoxometalate-Catalyzed Reactions. *Chem. Rev.* **2015**, *115*, 4893-4962; (c) Bijelic, A.; Aureliano, M.; Rompel, A., Polyoxometalates as Potential Next-Generation Metallodrugs in the Combat Against Cancer. *Angew. Chem. Int. Ed. Engl.* **2019**, *58*, 2980-2999; (d) Chen, L.; Chen, W. L.; Wang, X. L.; Li, Y. G.; Su, Z. M.; Wang, E. B., Polyoxometalates in dye-sensitized solar cells. *Chem. Soc. Rev.* **2019**, *48*, 260-284.

(3) (a) Döbereiner, J. W., Vermischte chemische Erfahrungen über Platin, Gährungschemie, usw. *Journal für Chemie und Physik*. **1828**, *54*, 412-426; (b) Goloboy, J. C.; Klemperer, W. G., Are Particulate Noble-Metal Catalysts Metals, Metal Oxides, or Something In-Between? *Angew. Chem. Int. Ed.* **2009**, *48*, 3562-3564.

(4) (a) Pley, M.; Wickleder, M. S., The cluster ion $[Pt^{12}O_8(SO_4)_{12}]^{4-}$. *Angew. Chem. Int. Ed.* **2004**, *43*, 4168-4170; (b) Rajan, A.; Elcheikh Mahmoud, M.; Wang, F.; Bhattacharya, S.; Mougharbel, A. S.; Ma, X.; Müller, A. B.; Nisar, T.; Taffa, D. H.; Poblet, J. M.; Kuhnert, N.; Wagner, V.; Wark, M.; Kortz, U., Discovery of Polythioplatinate(II) $[Pt_3S_2(SO_3)_6]^{10-}$ and Study of Its Solution and Catalytic Properties. *Inorg. Chem*. **2022**, *61*, 11529-11538. Reaction conditions used in this work: a feed flow rate of 0.05 mL/min (hydrogen flow rate = 22.5 mL_n/min and P_{H_2} = 28 bar).

(5) (a) Chubarova, E. V.; Dickman, M. H.; Keita, B.; Nadjo, L.; Miserque, F.; Mifsud, M.; Arends, I. W. C. E.; Kortz, U., Self-Assembly of a Heteropolyoxopalladate Nanocube: $[Pd^{II}_{13}As^{V}_8O_{34}(OH)_6]^{8-}$. *Angew. Chem. Int. Ed.* **2008**, *47*, 9542-9546; (b) Izarova, N. V.; Vankova, N.; Heine, T.; Biboum, R. N.; Keita, B.; Nadjo, L.; Kortz, U., Polyoxometalates Made of Gold: The Polyoxoaurate $[Au^{III}_4As_4O_{20}]^{8-}$. *Angew. Chem. Int. Ed.* **2010**, *49*, 1886-1889; (c) Izarova, N. V.; Vankova, N.; Banerjee, A.; Jameson, G. B.; Heine, T.; Schinle, F.; Hampe, O.; Kortz, U., A Noble-Metalate Bowl: The Polyoxo-6-vanado(V)-7-palladate(II) $[Pd_7V_6O_{24}(OH)_2]^{6-}$. *Angew. Chem. Int. Ed. Engl.* **2010**, *49*, 7807-7811; (d) Barsukova-Stuckart, M.; Izarova, N. V.; Jameson, G. B.; Ramachandran, V.;

Wang, Z.; van Tol, J.; Dalal, N. S.; Biboum, R. Ngo; Keita, B.; Nadjo, L.; Kortz, U., Synthesis and Characterization of the Dicopper(II)-Containing 22-Palladate(II) $[Cu^{II}_2Pd^{II}_{22}P^{V}_{12}O_{60}(OH)_8]^{20-}$. *Angew. Chem. Int. Ed. Engl.* **2011**, *50*, 2639-2642; (e) Barsukova-Stuckart, M.; Izarova, N. V.; Barrett, R.; Wang, Z.; van Tol, J.; Kroto, H. W.; Dalal, N. S.; Keita, B.; Heller, D.; Kortz, U., 3d Metal Ions in Highly Unusual Eight-Coordination: The Phosphate-Capped Dodecapalladate(II) Nanocube. *Chem. Eur. J.* **2012**, *18*, 6167-6171; (f) Yang, P.; Xiang, Y.; Lin, Z.; Bassil, B. S.; Cao, J.; Fan, L.; Fan, Y.; Li, M. X.; Jimenez-Lozano, P.; Carbo, J. J.; Poblet, J. M.; Kortz, U., Alkaline Earth Guests in Polyoxopalladate Chemistry: From Nanocube to Nanostar via an Open-Shell Structure. *Angew. Chem. Int. Ed. Engl.* **2014**, *53*, 11974-11978; (g) Yang, P.; Kortz, U., Discovery and Evolution of Polyoxopalladates. *Acc. Chem. Res.* **2018**, *51*, 1599-1608; (h) Xu, F.; Miras, H. N.; Scullion, R. A.; Long, D. L.; Thiel, J.; Cronin, L. L., Correlating the magic numbers of inorganic nanomolecular assemblies with a $\{Pd_{84}\}$ molecular-ring Rosetta Stone. *Proc. Natl. Acad. Sci. USA.* **2012**, *109*, 11609-11612.

(6) (a) Bhattacharya, S.; Basu, U.; Haouas, M.; Su, P.; Espenship, M. F.; Wang, F.; Sole-Daura, A.; Taffa, D. H.; Wark, M.; Poblet, J. M.; Laskin, J.; Cadot, E.; Kortz, U., Discovery and Supramolecular Interactions of Neutral Palladium-Oxo Clusters Pd_{16} and Pd_{24}. *Angew. Chem. Int. Ed. Engl.* **2021**, *60*, 3632-3639; (b) Bhattacharya, S.; Ma, X.; Mougharbel, A. S.; Haouas, M.; Su, P.; Espenship, M. F.; Taffa, D. H.; Jaensch, H.; Bons, A. J.; Stuerzer, T.; Wark, M.; Laskin, J.; Cadot, E.; Kortz, U., Discovery of a Neutral 40-Pd^{II}-Oxo Molecular Disk, $[Pd_{40}O_{24}(OH)_{16}\{(CH_3)_2AsO_2\}_{16}]$: Synthesis, Structural Characterization, and Catalytic Studies. *Inorg. Chem.* **2021**, *60*, 17339-17347.

(7) Bhattacharya, S.; Barba-Bon, A.; Zewdie, T. A.; Müller, A. B.; Nisar, T.; Chmielnicka, A.; Rutkowska, I. A.; Schurmann, C. J.; Wagner, V.; Kuhnert, N.; Kulesza, P. J.; Nau, W. M.; Kortz, U., Discrete, Cationic Palladium(II)-Oxo Clusters via f-Metal Ion Incorporation and their Macrocyclic Host-Guest Interactions with Sulfonatocalixarenes. *Angew. Chem. Int. Ed. Engl.* **2022**, *61*, e202203114.

(8) (a) Privalov, V. I.; Lapkin, V. V.; Tarasov, V. P.; Buslaev, Y. A., ^{195}Pt, ^{15}N NMR spectroscopy of aqueous solutions of mixed valent oxonitrocomplexes, Pt(II,IV): $K_5[(NO_2)_3Pt^{IV}(\mu\text{-}O)^3Pt^{II}_3(NO_2)_6]$ and $K_8[(NO_2)_6Pt^{II}_3(\mu\text{-}O)_3Pt^{IV}(\mu\text{-}O)_3Pt^{II}_3(NO_2)_6]$. *Appl. Magn. Reson.* **1990**, *1*, 445-456; (b) Min, D.;

Larsen, R. D.; Emerson, K.; Abbott, E. H., Synthesis and Crystal and Molecular Structures of Potassium Bis(μ-hydroxo) bis[dinitritoplatinate(II)] Sesquihydrate and Potassium *cyclo*-Tris(μ_3-oxo- l:2:4;l:3:4;2:3:4)tris[dinitritoplatinate(II)]trinitritoplatinate(IV) Trihydrate. *Inorg. Chem.* **1990**, *29*, 73-76.

(9) Vasilchenko, D.; Berdugin, S.; Tkachev, S.; Baidina, I.; Romanenko, G.; Gerasko, O.; Korenev, S., Polynuclear Hydroxido-Bridged Complexes of Platinum(IV) with Terminal Nitrato Ligands. *Inorg. Chem.* **2015**, *54*, 4644-4651.

(10) (a) Lee, U.; Kobayashi, A.; Sasaki, Y., Structure of Pentasodium Trihydrogenhexatungstoplatinate(IV) Icosahydrate, $Na_5[H_3PtW_6O_{24}]\cdot 20H_2O$. *Acta. Cryst.* **1983**, *C39*, 817-819; (b) Lee, U.; Sasaki, Y. Isomerism of the hexamolybdo-platinate (IV) polyanion. Crystal structures of $K_{3.5}[\alpha\text{-}H_{4.5}PtMo_6O_{24}]\cdot 3H_2O$ and $[NH_4]_4[\beta\text{-}H_4PtMo_6O_{24}]\cdot 1.5H_2O$. *Chem. Lett.* **1984**, 1297-1300.

(11) Lee, U.; Joo, H. C.; Park, K. M.; Mal, S. S.; Kortz, U.; Keita, B.; Nadjo, L., Facile incorporation of platinum(IV) into polyoxometalate frameworks: preparation of $[H_2Pt^{IV}V_9O_{28}]^{5-}$ and characterization by ^{195}Pt NMR spectroscopy. *Angew. Chem. Int. Ed.* **2008,** *47*, 793-796.

(12) Abramov, P. A.; Vicent, C.; Kompankov, N. B.; Gushchin, A. L.; Sokolov, M. N., Platinum polyoxoniobates. *Chem. Commun.* **2015**, *51*, 4021-4023.

(13) Sokolov, M. N.; Adonin, S. A.; Peresypkina, E. V.; Fedin, V. P., A Pt(II) isopolytungstate: synthesis and crystal structure. *Dalton. Trans.* **2012**, *41*, 11978-11979.

(14) (a) Kato, M.; Kato, C. N., A Keggin-type polyoxotungstate-coordinated diplatinum(II) complex: Synthesis, characterization, and stability of the cis-platinum(II) moieties in dimethylsulfoxide and water. *Inorg. Chem. Commun.* **2011**, *14*, 982-985; (b) Deng, W.; Zhang, Q.; Wang, Y., Polyoxometalates as efficient catalysts for transformations of cellulose into platform chemicals. *Dalton. Trans.* **2012**, *41*, 9817-9831.

(15) Lin, Z.; Izarova, N. V.; Kondinski, A.; Xing, X.; Haider, A.; Fan, L.; Vankova, N.; Heine, T.; Keita, B.; Cao, J.; Hu, C.; Kortz, U., Platinum-Containing Polyoxometalates: syn- and anti-$[Pt^{II}2(\alpha\text{-}PW_{11}O_{39})_2]^{10-}$ and Formation of the Metal-Metal-Bonded di-Pt(III) Derivatives. *Chem. Eur. J.* **2016**, *22*, 5514-5519.

(16) Kato, C. N.; Nagatani, S.; Mizuno, T., Synthesis, Characterization, and Stability of α-Keggin-Type Polyoxotungstate-Coordinated Mono-Platinum(II) Complex. *Eur. J. Inorg. Chem.* **2018**, *2019*, 517-522.

(17) Ma, X.; Bhattacharya, S.; Nisar, T.; Müller, A. B.; Wagner, V.; Kuhnert, N.; Kortz, U. Mixed-Valent Palladium(IV/II)-Oxoanion, $[Pd^{IV}O_6Pd^{II}_6((CH_3)_2AsO_2)_6]^{2-}$. *Chem. Commun.* **2023**, *59*, 904-907.

(18) *APEX suite of crystallographic software*, *APEX 3*, *version 2015.5-2*, Bruker AXS Inc., Madison, Wisconsin, USA, **2015**.

(19) *CrysAlisPro Software System, Version 1.171.38.41*. Rigaku Oxford Diffraction.

(20) SAINT, Version 7.56a and SADABS Version 2008/1, Bruker AXS Inc., Madison, Wisconsin, USA, **2008**.

(21) ABSPACK, SCALE. "Empirical absorption correction." *CrysAlis Pro–Software Package*, Rigaku Oxford Diffraction, **2022**.

(22) Sheldrick, G. M., "*SHELXL-2014*", University of Göttingen, Göttingen, Germany, **2014**.

(23) Spek, A. L., *PLATON*, *A Multipurpose Crystallographic Tool*, Utrecht University, Utrecht, The Netherlands, **2010**.

(24) Brown, I. D., Altermatt, D., Bond-Valence Parameters Obtained from a Systematic Analysis of the Inorganic Crystal Structure Database. *Acta Crystallogr.* **1985**, *B41*, 244-247.

(25) (a) Zhao, D.; Feng, J.; Huo, Q.; Melosh, N.; Fredrickson, G. H.; Chmelka, B. F.; Stucky, G. D., Triblock Copolymer Syntheses of Mesoporous Silica with Periodic 50 to 300 Angstrom Pores. *Science*, **1998**, *279*, 548-552; (b) Zhao, D.; Huo, Q.; Feng, J.; Chmelka, B. F.; Stucky, G. D., Nonionic Triblock and Star Diblock Copolymer and Oligomeric Surfactant Syntheses of Highly Ordered, Hydrothermally Stable, Mesoporous Silica Structures. *J. Am. Chem. Soc*. **1998**, *120*, 6024-6036.

(26) (a) Lee, C.; Yang, W.; Parr, R. G., Development of the Colle-Salvetti correlation-energy formula into a functional of the electron density, *Phys. Rev. B*, **1988**, *37*, 785-789; (b) Becke, A. D., Density-functional thermochemistry. I. The effect of the exchange-only gradient correction, *J. Chem. Phys.***1992**, *96*, 2155-2160.

(27) (a) Handy, N. C.; Cohen, A. J., Left-right correlation energy, *Mol. Phys*. **2001**, *99*, 403-412; (b)

Hoe, W.-M.; Cohen, A. J.; Handy, N. C. Assessment of a new local exchange functional OPTX, *Chem. Phys. Lett.* **2001**, *341*, 319-328; (c) Perdew, J. P.; Burke, K.; Ernzerhof, M., Generalized gradient approximation made simple, *Phys. Rev. Lett.* **1996**, *77*, 3865-3868.

(28) (a) Hehre, W. J.; Ditchfield, R.; Pople, J. A., Self-Consistent Molecular Orbital Methods. 12. Further extensions of Gaussian-type basis sets for use in molecular-orbital studies of organic-molecules, *J. Chem. Phys.* **1972**, *56*, 2257-2261; (b) Hariharan, P. C.; Pople, J. A., Influence of polarization functions on molecular-orbital hydrogenation energies, *Theor. Chem. Acc.* **1973**, *28*, 213-222; (c) Francl, M. M.; Pietro, W. J.; Hehre, W. J.; Binkley, J. S.; DeFrees, D. J.; Pople, J. A.; Gordon, M. S. Self-Consistent Molecular Orbital Methods. 23. A polarization-type basis set for 2nd-row elements, *J. Chem. Phys.* **1982**, *77*, 3654-3665.

(29) (a) Hay, P. J.; W. R. Wadt, Ab initio effective core potentials for molecular calculations - potentials for the transition-metal atoms Sc to Hg, *J. Chem. Phys.* **1985**, *82*, 270-83; (b) Wadt, W. R.; P. J. Hay, Ab initio effective core potentials for molecular calculations – potentials for main group elements Na to Bi, *J. Chem. Phys.* **1985**, *82*, 284-98.

(30) Cancès, E.; Mennucci, B.; Tomasi, J., A new integral equation formalism for the polarizable continuum model: Theoretical background and applications to isotropic and anistropic dielectrics, *J. Chem. Phys.* **1997**,*107*, 3032-3041.

(31) Gaussian 16, Revision A.03, Frisch, M. J.; Trucks, G. W.; Schlegel, H. B.; Scuseria, G. E.; Robb, M. A.; Cheeseman, J. R.; Scalmani, G.; Barone, V.; Petersson, G. A.; Nakatsuji, H.; Li, X.; Caricato, M.; Marenich, A. V.; Bloino, J.; Janesko, B. G.; Gomperts, R.; Mennucci, B.; Hratchian, H. P.; Ortiz, J. V.; Izmaylov, A. F.; Sonnenberg, J. L.; Williams-Young, D.; Ding, F.; Lipparini, F.; Egidi, F.; Goings, J.; Peng, B.; Petrone, A.; Henderson, T.; Ranasinghe, D.; Zakrzewski, V. G.; Gao, J.; Rega, N.; Zheng, G.; Liang, W.; Hada, M.; Ehara, M.; Toyota, K.; Fukuda, R.; Hasegawa, J.; Ishida, M.; Nakajima, T.; Honda, Y.; Kitao, O.; Nakai, H.; Vreven, T.; Throssell, K.; Montgomery, J. A., Jr.; Peralta, J. E.; Ogliaro, F.; Bearpark, M. J.; Heyd, J. J.; Brothers, E. N.; Kudin, K. N.; Staroverov, V. N.; Keith, T. A.; Kobayashi, R.; Normand, J.; Raghavachari, K.; Rendell, A. P.; Burant, J. C.; Iyengar, S. S.; Tomasi, J.; Cossi, M.; Millam, J. M.; Klene, M.; Adamo, C.; Cammi, R.; Ochterski, J. W.; Martin, R. L.; Morokuma, K.; Farkas, O.; Foresman, J. B.; Fox, D. J. Gaussian, Inc., Wallingford CT, 2016.

(32) ADF 2019.306, SCM, Theoretical Chemistry, Vrije Universiteit, Amsterdam, The Netherlands, http://www.scm.com.

(33) Van Lenthe, E. and Baerends, E. J., Optimized Slater-type basis sets for the elements 1–118. J. *Comput. Chem.* **2003**, *24*, 1142-1156.

(34) Van Lenthe, E.; Baerends, E. J.; Snijders, J. G., Relativistic regular two-component Hamiltonians. *J. Chem. Phys.* **1993**, *99* (6), 4597-4610.

(35) Pye, C. C.; Ziegler, T., An implementation of the conductor-like screening model of solvation within the Amsterdam density functional package, *Theor. Chem. Acc.* **1999**, *101*, 396-408.

(36) Autschbach, J., Magnitude of Finite-Nucleus-Size Effects in Relativistic Density Functional Computations of Indirect NMR Nuclear Spin–Spin Coupling Constants. *Chem. Phys. Chem.* **2009**, *10*, 2274-2283.

(37) (a) Pascual-Borràs, M.; López, X.; Rodríguez-Fortea, A.; Errington, R. J.; Poblet, J. M. ^{17}O NMR Chemical Shifts in Oxometalates: From the Simplest Monometallic Species to Mixed-Metal Polyoxometalates. *Chem. Sci.* **2014**, *5*, 2031; (b) Kondinski, A.; Vankova, N.; Schinle, F.; Jäger, P.; Hampe, O.; Kortz, U.; Heine, T. How Counterions Affect the Solution Structure of Polyoxoaurates: Insights from UV/Vis Spectral Simulations and Electrospray Mass Spectrometry. *Eur. J. Inorg. Chem.* **2014**, 3771-3778; (c) Pascual-Borràs, M.; López, X.; Poblet, J. M. Accurate Calculation of 31P NMR Chemical Shifts in Polyoxometalates. *Phys. Chem. Chem. Phys.* **2015**, *17*, 8723.

(38) Swart, M.; Solà, M.; Bickelhaupt, F. M., A new all-round density functional based on spin states and S_N2 barriers. *J. Chem. Phys.* **2009**, *131*(9), 094103.

(39) (a) Wiesenfeldt, M. P.; Nairoukh, Z.; Dalton, T.; Glorius, F., SelectiveArene Hydrogenation for Direct Access to Saturated Carbo- and Heterocycles. *Angew. Chem. Int. Ed*. **2019**, *58*, 10460-10476; (b) Zhang, L.; Zhou, M.; Wang, A.; Zhang, T., Selective Hydrogenation over Supported Metal Catalysts: From Nanoparticles to Single Atoms. *Chem. Rev*. **2020**, *120*, 683-733; (c) Gao, C.; Lyu, F.; Yin, Y., Encapsulated Metal Nanoparticles for Catalysis. *Chem. Rev*. **2021**, *121*, 834-881.

(40) (a) Chakraborty, I.; Pradeep, T., Atomically Precise Clusters of Noble Metals: Emerging Link between Atoms and Nanoparticles. *Chem. Rev*. **2017**, *117*, 8208-8271; (b) Du, Y.; Sheng, H.;

Astruc, D.; Zhu, M., Atomically Precise Noble Metal Nanoclusters as Efficient Catalysts: A Bridge between Structure and Properties. *Chem. Rev*. **2020**, *120*, 526-622.

(41) Wang, Q.-M.; Lin, Y.-M.; Liu, K.-G., Role of Anions Associated with the Formation and Properties of Silver Clusters. *Acc. Chem. Res*. **2015**, *48*, 1570-1579.

(42) Stanislaus, A.; Cooper, B. H., Aromatic Hydrogenation Catalysis: A Review. *Catal. Rev.: Sci. Eng*. **1994**, *36*, 75-123.

(43) Ayass, W. W.; Minambres, J. F.; Yang, P.; Ma, T.; Lin, Z.; Meyer, R.; Jaensch, H.; Bons, A. J.; Kortz, U., Discrete Polyoxopalladates as Molecular Precursors for Supported Palladium Metal Nanoparticles as Hydrogenation Catalysts. *Inorg. Chem.* **2019**, *58*, 5576-5582.

(44) Wang, J.; Huang, L.; Li, Q., Influence of different diluents in Pt/Al_2O_3 catalyst on the hydrogenation of benzene, toluene and *o*-xylene. *Applied Catalysis A: General*, **1998**, *175*, 191-199. Reaction conditions used in this work: a stainless steel tube with 4 mm i.d. at a pressure of 2.2 bars with the flow rate of hydrogen, the carrier gas, always being 50 mLmin.

(45) Wu, Y.; Chai, Y.; Li, J.; Guo, H.; Wen, L.; Liu, C., Preparation of silicalite-1@Pt/alumina core–shell catalyst for shape-selective hydrogenation of xylene isomers. *Catalysis Communications*, **2015**, *64*, 110-113. Reaction conditions used in this work: 1.0 MPa,W_{cat} =2 g, feed=4 mL/h, hydrogen flow rate =2400 mL/h.

(46) Letellier, F.; Blanchard, J.; Fajerwerg, K.; Louis, C.; Breysse, M.; Guillaume, D.; Uzio, D., Search for confinement effects in mesoporous supports: hydrogenation of *o*-xylene on Pt°/MCM-41. *Catalysis Letters*, **2006**, *110*, 115-124. Reaction conditions used in this work: P = 1 atm, 5% *o*-x/*n*-C_7 vol., [H_2]/[*o*-xylene] = 10 molar ratio.

(47) (a) Viniegra, M.; Córdoba, G.; Gómez, R., Gas phase hydrogenation of o-xylene over palladium catalysts, *J. Mol. Catal.* **1990**, *58*, 107; (b) Saymeh, R. A.; Asfour, H. M.; Tuaimen, W. A., Gas phase study of *o*-xylene hydrogenation over Pt/Al_2O_3: Influence of the catalyst reduction temperature on selectivity, *Asian J. Chem.* **1997**, *9*, 350; (c) Neyestanaki, A. K.; Mäki-Arvela, P.; Backman, H.; Karhu, H.; Salmi, T.; Väyrynen, J.; Murzin, D. Y., Kinetics and stereoselectivity of o-xylene hydrogenation over Pd/Al_2O_3, *Journal of Molecular Catalysis A: Chemical*, **2003**, *193*, 237-250.

(48) Menon, P. G., Diagnosis of Industrial Catalyst Deactivation by Surface Characterization

Techniques, *Chem. Rev.* **1994**, *94*, 1021-1046.

(49) Peck, J. W.; Koel, B. E., Selective Dehydrogenation of 1,3-Cyclohexadiene on Ordered Sn/Pt(111) Surface Alloys, *J. Am. Chem. Soc.* **1996**, *118*, 2708.

(50) Inuone, Y.; Herrmann, J. M.; Schmidt, H.; Burwell, R. L.; Butt, J. B.; Cohen, J. B., $PtSiO_2$: IV. Isotopic exchange between cyclopentane and deuterium, *J. Catal.* **1978**, *53*, 401.

TOC text and figure

The first mixed-valent Pt^{IV}-centered hexaplatinate(II) $[Pt^{IV}Pt^{II}_6O_6(AsO_2(CH_3)_2)_6]^{2-}$ (**Pt$_7$**) and the Pt^{IV}-centered hexapalladate(II) $[Pt^{IV}Pd^{II}_6O_6(AsO_2(CH_3)_2)_6]^{2-}$ (**PtPd$_6$**) have been prepared and characterized in the solid-state, in solution, and in the gas phase.